

 Open access • Journal Article • DOI:10.1021/LA802323X

Linear-to-branched micelles transition: a rheometry and diffusing wave spectroscopy (DWS) study. — [Source link](#)

Claude Oelschlaeger, M. Schopferer, Frank Scheffold, Norbert Willenbacher

Institutions: University of Fribourg

Published on: 20 Jan 2009 - Langmuir (American Chemical Society)

Topics: Shear modulus, Diffusing-wave spectroscopy, Rheometry and Microrheology

Related papers:

- [Statics and dynamics of worm-like surfactant micelles](#)
- [Wormlike micelles: where do we stand? Recent developments, linear rheology and scattering techniques](#)
- [Stress relaxation in living polymers: Results from a Poisson renewal model](#)
- [Effect of counterion binding efficiency on structure and dynamics of wormlike micelles.](#)
- [Reptation of living polymers: dynamics of entangled polymers in the presence of reversible chain-scission reactions](#)

Share this paper:    

View more about this paper here: <https://typeset.io/papers/linear-to-branched-micelles-transition-a-rheometry-and-47uy9vmyy6>

Linear-to-Branched Micelles Transition: A Rheometry and Diffusing Wave Spectroscopy (DWS) Study

C. Oelschlaeger,^{*,†} M. Schopferer,[†] F. Scheffold,[‡] and N. Willenbacher[†]

Institute of Mechanical Process Engineering and Mechanics, University Karlsruhe, Gotthard-Franz-Str. 3, 76128 Karlsruhe, Germany, and Department of Physics, University of Fribourg, 1700 Fribourg Perolles, Switzerland

Received July 25, 2008. Revised Manuscript Received October 1, 2008

The frequency-dependent shear modulus of aqueous wormlike micellar solutions of cetylpyridinium chloride (CPyCl) and sodium salicylate (NaSal) has been measured over a broad frequency range from 10^{-2} to 10^6 rad/s using diffusing wave spectroscopy (DWS) based tracer microrheology as well as mechanical techniques including rotational rheometry and oscillatory squeeze flow. Good agreement between mechanical and optical techniques is found in the frequency range from 10^{-1} to 10^5 rad/s (Willenbacher, N.; Oelschlaeger, C.; Schopferer, M.; Fischer, P.; Cardinaux, F.; Scheffold, F. *Phys. Rev. Lett.* **2007**, *99* (6), 068302). At intermediate frequencies between 10 and 10^4 rad/s, squeeze flow provides most accurate data and is used to determine the plateau modulus G_0 , which is related to the cross-link density or mesh size of the entanglement network, as well as the scission energy E_{sciss} , which is deduced from the temperature dependence of the shear moduli in the plateau zone. In the frequency range above 10^4 rad/s, DWS including a new inertia correction is most reliable and is used to determine the persistence length l_p . The system CPyCl/NaSal is known to exhibit two maxima in zero-shear viscosity and terminal relaxation time as the salt/surfactant ratio R is varied (Rehage, H.; Hoffman, H. *J. Phys. Chem.* **1988**, *92* (16), 4712–4719). The first maximum is attributed to a transition from linear to branched micelles (Lequeux, F. *Europhys. Lett.* **1992**, *19* (8), 675–681), and the second one is accompanied by a charge reversal due to strongly binding counterions. Here, we discuss the variation of G_0 , E_{sciss} , and l_p with salt/surfactant ratio R at constant surfactant concentration of 100 mM CPyCl. G_0 increases at the linear-to-branched micelles transition, and this is attributed to the additional contribution of branching points to the cross-link density. E_{sciss} exhibits two maxima analogous to the zero-shear viscosity, which can be understood in terms of the variation of micellar length and variation of the amount of branched micelles and contour length between branching points consistent with the results of a comprehensive cryo-transmission electron microscopy (TEM) study (Abezgaux, L.; Ramon, O.; Danino, D. Department of Biotechnology and Food Engineering, Technion, Haifa, Israel. European Colloid and Interface Society, Geneva, 2007). The persistence length decreases with increasing R . This decrease is stronger than expected from the decrease of Debye length according to the Odijk–Skolnick–Fixman (OSF) theory and is attributed to the penetration of salicylate ions into the micelles; the linear-to-branched transition obviously does not have an effect on l_p .

1. Introduction

In solution, amphiphilic surfactant molecules can self-assemble to form various structures such as spherical or wormlike micelles, vesicles, or hexagonal and lamellar liquid crystalline structures. These different aggregation structures can show distinct rheological properties. Surfactant solutions with wormlike micellar structures are widely used in home and personal care products as well as enhanced oil recovery but also as drag reduction agents in district heating systems or most recently as templates for asymmetric and aligned nanostructures as well as sieving matrix for separation of DNA fragments.^{5,6} The structural and rheological properties of wormlike micelles (WLMs) have been investigated intensively not only because of their wide application range, but also because they show many analogies to covalently bonded polyelectrolytes and can be used as model systems to study the structure and dynamics of polymers. Since micelles break and reform (rate constant k), they are often termed “equilibrium” or

“living” polymers. Small changes in surfactant structure, counterion type and concentration, added electrolytes, or temperature can alter the length, flexibility, and interactions of micelles, drastically resulting in pronounced effects on macroscopic rheological properties. In particular, various ionic surfactants show a pronounced maximum of the zero-shear viscosity as the salt/surfactant ratio is varied.^{7–11} This is of significant interest from an application point of view, since this viscosity maximum is closely related to the application properties of corresponding surfactant systems, but also from a scientific point of view, since the structural changes corresponding to this viscosity maximum are still not really clear. Several studies support the transition from linear to branched micelles: for example, a combined cryo-transmission electron microscopy (TEM), small-angle neutron scattering (SANS), and rheology study on the system erucyl-bis(hydroxyethyl)methylammonium chloride (EHAC)/KCl consistently revealed a transition from linear to branched micelles around the viscosity maximum.¹² In contrast to ordinary polymers, these branch points can slide along the micelles and hence provide

[†] University Karlsruhe.

[‡] University of Fribourg.

(1) Willenbacher, N.; Oelschlaeger, C.; Schopferer, M.; Fischer, P.; Cardinaux, F.; Scheffold, F. *Phys. Rev. Lett.* **2007**, *99*(6), 068302.

(2) Rehage, H.; Hoffman, H. *J. Phys. Chem.* **1988**, *92*(16), 4712–4719.

(3) Lequeux, F. *Europhys. Lett.* **1992**, *19*(8), 675–681.

(4) Abezgaux, L.; Ramon, O.; Danino, D. Department of Biotechnology and Food Engineering, Technion, Haifa, Israel. European Colloid and Interface Society, Geneva, 2007.

(5) Walker, L. M. *Curr. Opin. Colloid Interface Sci.* **2001**, *6*(5–6), 451–456.

(6) Yang, J. *Curr. Opin. Colloid Interface Sci.* **2002**, *7*(5–6), 276–281.

(7) Candau, S. J.; Khatory, A.; Lequeux, F.; Kern, F. *J. Phys. IV* **1993**, *3*, 197–209.

(8) Cappelare, E.; Cressely, R. *Colloid Polym. Sci.* **1998**, *276*, 1050–1056.

(9) Cappelare, E.; Cressely, R. *Rheol. Acta* **2000**, *39*, 346–353.

(10) Raghavan, S. R.; Kaler, E. W. *Langmuir* **2001**, *17*, 300–306.

(11) Schubert, B. A.; Kaler, E. W.; Wagner, N. J. *Langmuir* **2003**, *19*, 4079–4089.

(12) Croce, V.; Cosgrove, T.; Maitland, G.; Hughes, T.; Karlsson, G. *Langmuir* **2003**, *19*, 8536–8541.

69 a high number of degrees of freedom for reptation resulting in
70 the observed viscosity reduction. In contrast, for the system cetyl
71 triammonium chloride (CTAC) and sodium salicylate (NaSal),
72 cryo-TEM images did not reveal significant branching around
73 the viscosity maximum and the viscosity drop was attributed to
74 a change in micellar breakage time.¹⁴ For the systems cetyl
75 triammonium bromide (CTAB)^{14,15} and cetyl pyridinium chloride
76 (CPyCl) with NaSal as strongly binding counterion,² even a
77 second viscosity maximum is observed when the salt concentra-
78 tion is further increased, but the underlying structural or dynamic
79 change of the system has not been resolved yet. In this study,
80 we use a recently established experimental approach¹ combining
81 mechanical high frequency rheology and optical microrheology
82 to get new insight into structural and dynamic changes ac-
83 companying the characteristic viscosity maxima observed in the
84 CPyCl/NaSal system at characteristic surfactant-to-salt ratios R .
85 The newly established approach gives access to the linear
86 viscoelastic properties of these solutions at frequencies up to 1
87 MHz. We investigate the dependence of the plateau modulus G_0 ,
88 the scission energy E_{sciss} , and the persistence length l_p with salt/
89 surfactant ratio R at constant surfactant concentration of 100
90 mM CPyCl. On the one hand, despite the large amount of literature
91 for this system, no results on the scission energy and bending
92 stiffness are available so far. On the other hand, this system is
93 particularly suited for the proposed study, since it has been shown
94 that there is good agreement between mechanical rheometry data
95 and optical microrheology^{1,16} in a very broad frequency range,
96 and thus, the high frequency linear viscoelastic properties can
97 be characterized thoroughly.

2. Relationship between Dynamical and Structural Features of Entangled Wormlike Micellar Solutions

100 Long and flexible linear micelles, commonly referred to as
101 “wormlike” micelles, can be described by a number of structural
102 parameters, which cover a broad range of length scales. The
103 overall length of the micelles is referred to as the contour length
104 L and varies from a few nanometers to micrometers. A mean
105 field treatment of the growth process for highly screened micelles
106 has been obtained from the models derived by Cates^{17–19} and
107 predicts an exponential distribution of length $N(L)$:

$$108 \quad N(L) \propto \exp\left(-\frac{L}{\bar{L}}\right) \quad (1)$$

109 with the average length given by

$$110 \quad \bar{L} \cong \varphi^{0.5} \exp\left(\frac{E_{\text{sciss}}}{2k_B T}\right) \quad (2)$$

111 where φ is the surfactant volume fraction, T is the temperature,
112 and E_{sciss} is the scission energy of the micelle, that represents the
113 excess free energy for a pair of hemispherical end-caps relative
114 to a rodlike region containing an equal number of surfactants.
115 Slight changes in the composition of surfactant solutions are
116 expected to affect their overall length, which is directly related
117 to the scission energy. In the present study, we investigate the

(13) Clausen, T.; Vinson, P. K.; Minter, J. R.; Davis, H. T.; Talmon, Y.; Miller, W. G. *J. Phys. Chem.* **1992**, 96(1), 474–484.

(14) Nemoto, N.; Kuwahara, M.; Yao, M.-L.; Osaki, K. *Langmuir* **1995**, 11, 30–36.

(15) Galvan-Miyoshi, J.; Delgado, J.; Castillo, R. *Eur. Phys. J. E.* **2008**, 26(4), 369–377.

(16) Buchanan, M.; Atakhorrami, M.; Palierno, J. F.; Schmidt, C. F. *Macromolecules* **2005**, 38, 8840–8844.

(17) Cates, M. E. *J. Phys. (Paris)* **1988**, 49, 1593.

(18) Cates, M. E. *Macromolecules* **1987**, 20, 2289.

(19) Israclachvili, J.; Mitchell, D. J.; Ninham, B. W. *J. Chem. Soc., Faraday Trans. 2* **1976**, 72, 1525.

118 influence of the scission energy on the dynamics and structure
119 of micellar solutions. For charged systems, this quantity has two
120 contributions:

$$121 \quad E_{\text{sciss}} = E_c - E_e \quad (3)$$

122 E_c is the energy required to create two hemispherical end-caps
123 as a result of scission of the wormlike micelles and reflects the
124 differences in surfactant packing in the end-caps versus the
125 cylindrical body of the micelles. For nonionic micelles or for
126 ionic micelles at high ionic strength, $E_{\text{sciss}} = E_c$. For ionic micelles,
127 repulsion between charged head groups favors micelle breaking
128 and lowers E_{sciss} ; this effect is summarized in E_e . According to
129 the theory of Cates and Granek,⁵⁷ the scission energy E_{sciss} is
130 related to the temperature dependence of the moduli G' and G''
131 at intermediate frequencies, in the so-called entanglement regime,
132 where G' exhibits a plateau and G'' ($\ll G'$) goes through a
133 minimum (in so-called Cole–Cole plots, significant deviations
134 occur from the semicircular shape expected for Maxwell fluids).
135 In this regime, the ratio G''_{min}/G_0 is related to l_e (contour length
136 between two successive entanglements) and \bar{L} according to⁵⁷

$$137 \quad \frac{G''_{\text{min}}}{G_0} \sim \frac{l_e}{\bar{L}} \sim \varphi^{-1.85} \exp\left(-\frac{E_{\text{sciss}}}{2k_B T}\right) \quad (4)$$

138 In the case of formation of branched micelles which correspond
139 to the formation of equilibrium cross-links arising through local
140 fusion of micelles, a model based on the coupled reptation/
141 reaction for branched micelles was developed by Lequeux.³ In
142 the frame of this model, all the results concerning the rheology
143 of linear wormlike micelles can be applied to branched micelles,
144 provided that one substitutes \bar{L} by \bar{L}_c , where \bar{L}_c represents the
145 harmonic mean between the average distance from one point
146 along the micelle to the first cross-link and the average distance
147 from that point to the first end-cap. Consequently, we determine
148 the scission energy using the same method (section 4.2.2) for
149 linear as well as for branched micelles. Another key structural
150 parameter for wormlike micellar solutions investigated here is
151 the plateau modulus G_0 . This parameter, determined at inter-
152 mediate frequencies, is directly related to the mesh size ξ of the
153 system with $G_0 \sim \xi^{-3}$ and is typically independent of temperature.¹
154 We also investigate the high frequency range; in this regime, the
155 stress relaxation, for linear micelles as well as for branched
156 micelles, is controlled by the internal dynamics of short micelle
157 segments and the moduli G' and G'' show characteristic scaling
158 behavior.

$$159 \quad G' \sim G'' \sim \omega^\alpha \quad (5)$$

160 First, the Rouse–Zimm modes dominate and $\alpha = 1/2 - 2/3$.

161 At even higher frequencies, internal bending modes of single
162 Kuhn segments determine G' and G'' , and hence, these dynamic
163 parameters are related to the bending modulus κ as a structural
164 parameter; κ is often expressed in terms of the persistence length
165 $\kappa = k_B T/l_p$. In this frequency range, the scaling exponent $\alpha =$
166 $3/4$ as predicted by Morse,²⁰ and Gittes and MacKintosh.²¹

167 The transition between these scaling regimes is marked by the
168 inverse of the shortest Rouse relaxation time $\omega_0 = \tau_0^{-1}$ which
169 is directly related to the persistence length l_p .

$$170 \quad \omega_0 = \frac{k_B T}{8\eta_s l_p} \quad (6)$$

171 where η_s is the solvent viscosity.

(20) Morse, D. C. *Phys. Rev. E* **1998**, 58(2), R1237–R1240.

(21) Gittes, F.; MacKintosh, F. C. *Phys. Rev. E* **1998**, 58(2), R1241–R1244.

172 The persistence length l_p can also be determined from the
173 absolute values of G' and G'' in the $\alpha = 3/4$ scaling regime
174 according to a relationship based on a statistical mechanical
175 treatment of the single filament stress response of semiflexible
176 chains presented in ref 21:

$$G^* = \frac{\rho}{15} Kl_p \left(\frac{-2i\zeta}{K} \right) \omega^{\frac{3}{4}} - i\omega\eta_s \quad (7)$$

178 where ζ is the lateral drag coefficient and ρ is the area density
179 of micelles. The latter can be calculated as $\rho = \phi_{\text{surf}}/((\pi/4)d_{\text{mic}}^2)$
180 where ϕ_{surf} is the surfactant concentration (vol/vol) and $(\pi/4)d_{\text{mic}}^2$
181 is the cross-sectional area of the micelles. So far, l_p has been
182 determined using various scattering techniques including small-
183 angle neutron scattering (SANS)^{22–24} as well as static and
184 dynamic light scattering.^{14,25–27} Birefringence measurements
185 can also be used to determine l_p .²⁸ Recently, it has been
186 demonstrated that also another neutron scattering technique,
187 namely, neutron spin echo (NSE), can be used to determine the
188 persistence length.²⁹ Robust and reliable models are available to
189 analyze scattering data, and SANS is a well established tool to
190 characterize wormlike micelles. However, limited access to large
191 scale facilities hinders its broad application for systematic
192 investigations with careful parameter variation. Light scattering
193 techniques are suitable for stiff micelles ($l_p \approx 100$ nm) only, due
194 to the different q -range which is accessed. Birefringence
195 measurements require the knowledge of optical constants which
196 are often not known. Recently, we have demonstrated that the
197 high frequency range where the $\omega^{3/4}$ -scaling occurs can be
198 accessed by optical as well as mechanical rheometry. Accordingly,
199 these techniques can be used to determine l_p according to eqs 5
200 and 6 even for l_p values down to a few nm.¹ In order to improve
201 the quality of the DWS data and to increase the accessible
202 frequency range to the MHz range, a self-consistent inertia
203 correction has been introduced^{1,30–32} for the DWS data.

204 All these structural features, the characteristic length scales,
205 and the corresponding characteristic relaxation times strongly
206 depend not only on the chemical nature and concentration of the
207 surfactant or surfactant mixture under consideration, but also on
208 the nature and concentration of the counterion (binding vs
209 nonbinding) and the ionic strength of the solution. This has been
210 studied intensively not only by rheological experiments but also
211 by using electron microscopy and various scattering tech-
212 niques.^{11,28,33,34} Cryo-TEM, for example, has been used to
213 visualize entanglements, branching, and the semiflexible, worm-
214 like nature of the micelles directly.^{12,13,35–37}

215 In the first part of this paper, we establish the relationship
216 between dynamical and structural features of entangled solutions
217 of wormlike micelles and we compare results from mechanical

218 rheometry and optical microrheology. We focus on three different
219 parameters: plateau modulus, scission energy, and persistence
220 length. In the second part of the paper, we investigate the effect
221 of salt concentration on these three parameters for the system
222 CPyCl in the presence of NaSal.

223 3. Materials and Methods

224 **3.1. Sample Characteristics.** Aqueous solutions of surfactant/
225 counterion mixtures cetylpyridinium chloride/sodium salicylate
226 (CPyCl/NaSal) were used as model systems. CPyCl and NaSal were
227 both obtained from C. Roth. The sample solutions were prepared
228 by gently stirring the surfactant and salt in deionized water. For
229 equilibrium measurements, they were stored for at least 1 day at 20
230 °C. This solution exhibits a very strong viscoelastic response in the
231 temperature range between 20 and 40 °C.^{38,39}

232 **3.2. DWS Based Optical Microrheology.** The basic idea of
233 optical microrheology is to study the equilibrium thermal response
234 of small (colloidal) particles embedded in a material and thereby
235 obtain quantitative information about the macroscopic loss and storage
236 moduli, $G'(\omega)$ and $G''(\omega)$, over an extended range of frequencies.
237 The modern way of using this technique was introduced in the mid-
238 1990s when Mason and Weitz proposed a quantitative relation
239 between the tracer mean-squared displacement $\langle \Delta r^2(t) \rangle$ and the
240 complex shear modulus $G^*(\omega)$.⁴⁰ The Laplace transform of the
241 particle mean squared displacement $\langle \Delta r^2(i\omega) \rangle$ is related to the complex
242 modulus of the sample via a generalized Stokes–Einstein equation
243 (GSE):

$$G^*(\omega) = \frac{k_B T}{\pi a i \omega \langle \Delta r^2(i\omega) \rangle} = G'(\omega) + iG''(\omega) \quad (8)$$

244 Assuming that the complex fluid can be treated as an isotropic,
245 incompressible continuum around a sphere, this relation was later
246 confirmed theoretically.⁴¹ Under this condition, the GSE is valid
247 essentially for all cases of practical interest except for the limit of
248 ultrahigh frequencies where inertia effects start to play a role. At
249 times much shorter than 10^{-5} s, or frequencies well above $\omega = 10^5$
250 rad/s, inertia effects become significant.³⁰ This means that $\langle \Delta r^2(t) \rangle$
251 not only is given by the viscous (or viscoelastic) properties of the
252 medium as assumed above but is distorted by inertia effects at times
253 much shorter than 10^{-4} s. The goal is therefore to recover the motion
254 pattern one would observe in the absence of inertia effects. In order
255 to be able to access this interesting ultrahigh frequency regime, we
256 have recently introduced a simple (self-consistent) correction
257 scheme.¹ Previous studies on dense colloidal suspensions have shown
258 that the effective high frequency viscosity determines the influence
259 of fluid inertia.³¹ From the raw $G''(\omega)$ data, we determine the effective
260 high frequency viscosity of approximately 3 mPas from a fit to
261 the loss modulus $G''(\omega) = \eta(\omega)\omega$ in the regime $\omega = 10^5$ – 10^6 s⁻¹.
262 We then correct the particle mean square displacement for inertia
263 effects based on the theory of Hinch³² developed for the motion of
264 a sphere in a simple fluid with viscosity η . In a second iteration step,
265 we again fit the resulting loss modulus and repeat this procedure
266 several times. In our case, the correction factor attains its smallest
267 value of 0.7 for the shortest time analyzed $\tau = 5 \times 10^{-7}$ s.
268

269 For a quantitative interpretation of the raw experimental data
270 $\langle \Delta r^2(t) \rangle$, the Laplace transformation is the most critical part of the
271 analysis. To reduce truncation errors, we apply a procedure suggested
272 by Mason and co-workers. We estimate $\tilde{G}(s)$ by substituting $\langle \Delta r^2(t) \rangle$
273 into an algebraic Stokes–Einstein form:⁴²

(35) Lin, Z. *Langmuir* **1996**, *12*(7), 1729–1737.

(36) Bernheim-Groswasser, A.; Wachtel, E.; Talmon, Y. *Langmuir* **2000**, *16*(9), 4131–4140.

(37) Bernheim-Groswasser, A.; Zana, R.; Talmon, Y. *J. Phys. Chem. B* **2000**, *104*(51), 12192–12201.

(38) Rehage, H.; Hoffmann, H. *Mol. Phys.* **1991**, *74*, 933.

(39) Fischer, P.; Rehage, H. *Rheol. Acta* **1997**, *36*, 13.

(40) Mason, T. G.; Weitz, D. A. *Phys. Rev. Lett.* **1995**, *74*, 1250.

(41) Levine, A. J.; Lubensky, T. C. *Phys. Rev. E* **2001**, *63*, 1–4.

(22) Magid, L. J.; Han, Z.; Li, Z.; Butler, P. D. *J. Phys. Chem. B* **2000**, *104*(29), 6717–6727.

(23) Hoffmann, H.; Kalus, J.; Schwandner, B. *Ber. Bunsen-Ges.* **1987**, *91*, 99–106.

(24) Pedersen, J. S.; Laso, M.; Schurtenberger, P. *Phys. Rev. E* **1996**, *54*, R5917–5920.

(25) Brown, W.; Johansson, K.; Almgren, M. *J. Phys. Chem.* **1989**, *93*(15), 5888–5894.

(26) Imae, T. *J. Phys. Chem.* **1990**, *94*, 5953–5959.

(27) Buhler, E.; Munch, J. P.; Candau, S. J. *J. Phys. II* **1995**, *5*(6), 765–787.

(28) Shikata, T.; Dahman, S. J.; Pearson, D. S. *Langmuir* **1994**, *10*(10), 3470–3476.

(29) Nettesheim, F.; Wagner, N. J. *Langmuir* **2007**, *23*, 5267–5269.

(30) Weitz, D. A.; Pine, D. J.; Pusey, P. N.; Though, R. J. A. *Phys. Rev. Lett.* **1989**, *63*, 1747.

(31) Ladd, A. J. C.; Gang, H.; Zhu, J. X.; Weitz, D. A. *Phys. Rev. Lett.* **1995**, *74*, 318.

(32) Hinch, E. *J. Fluid Mech.* **1975**, *72*, 499.

(33) Cates, M. E.; Candau, S. J. *J. Phys.: Condens. Matter* **1990**, *2*, 6869–6892.

(34) Magid, L. J.; Li, Z.; Butler, P. D. *Langmuir* **2000**, *16*, 10028–10036.

$$\tilde{G}(s) = \frac{k_B T}{\pi a \langle \Delta r^2(t) \rangle \Gamma[1 + (\partial \ln \langle \Delta r^2(t) \rangle / \partial t)^{1/s}]} \quad (9)$$

274
275 In order to reduce scatter, we first fit $\langle \Delta r^2(t) \rangle$ with a polynomial of
276 order 6 or 7 and then use eq 9 to extract the moduli $G'(\omega)$ and $G''(\omega)$.
277 We have checked that the choice of the polynomial order and the
278 range of data selected do not influence the results. Finally, it is
279 worthwhile to note that, contrary to mechanical measurements, the
280 in- and out-of-phase contributions are not measured independently
281 but have to be extracted from a single value of the slope $\partial \ln \langle \Delta r^2(t) \rangle /$
282 ∂t . As a consequence, if $G'(\omega)$ and $G''(\omega)$ are of different magnitude,
283 the lower value extracted from DWS measurements is often not very
284 well defined.

285 A number of methods have been applied successfully to measure
286 the particle mean square displacement, notably single particle tracking
287 by microscopy, laser deflection, and diffusing wave spectroscopy
288 (DWS).^{43–45} In this work, we have chosen DWS as the only technique
289 that provides access to frequencies well above 10^4 rad/s. The DWS
290 technique is an extension of dynamic light scattering (DLS) to soft
291 materials exhibiting strong multiple scattering.⁴⁶ The method allows
292 one to monitor the displacement of micrometer sized colloidal
293 particles with subnanometer precision and on time scales as short
294 as 10 ns. In recent years, significant progress has been made in
295 development of the DWS approach, and it has been successfully
296 applied to the study of fluid and solid media, for example, colloidal
297 suspensions, gels, and biocolloids (yogurt and cheese) as well as
298 ceramic slurries and green bodies.^{47–50} In a DWS experiment,
299 coherent laser light impinges on one side of a turbid sample and the
300 intensity fluctuations of the light propagated through the sample are
301 then analyzed either in transmission or backscattering geometry. A
302 diffusion model is used to describe the propagation of photons across
303 the sample. Analogous to traditional dynamic light scattering (DLS),
304 for the case of noninteracting particles, it is possible to express the
305 measured intensity autocorrelation function (ICF) $g_2(\tau) - 1 = \langle I(t)$
306 $I(t + \tau) \rangle / \langle I \rangle^2 - 1$ in terms of the mean square displacement of the
307 scattering particle,

$$g_2(\tau) - 1 = \left[\int_0^\infty ds P(s) \exp(-s/l^* k^2 \langle \Delta r^2(\tau) \rangle) \right]^2 \quad (10)$$

308
309 with $k = 2\pi n/\lambda$ being the wavenumber of light in a medium with
310 refractive index n . $P(s)$ is the distribution of photon trajectories of
311 length s in the sample, and it can be calculated within the diffusion
312 model taking into account the experimental geometry. For the case
313 of transmission through a slab (plane-wave illumination), one obtains

$$g_2(\tau) - 1 = \left[\frac{(L/l^* + 4/3) \sqrt{\langle k_0^2 \Delta r^2(\tau) \rangle}}{\sinh[(L/l^* + 4/3) \sqrt{\langle k_0^2 \Delta r^2(\tau) \rangle}]} \right]^2 \quad (11)$$

314
315 The transport mean free path l^* characterizes the typical step
316 length of the photon random walk, given by the individual particle
317 scattering properties and particle concentration, and l^* can be
318 determined independently by a comparison of the measured count
319 rate to the one obtained with a sample of known l^* (ref 51) and
320 therefore enters the analysis as a constant parameter. Equation 11
321 numerically calculated the particle mean square displacement $\langle \Delta r^2(t) \rangle$

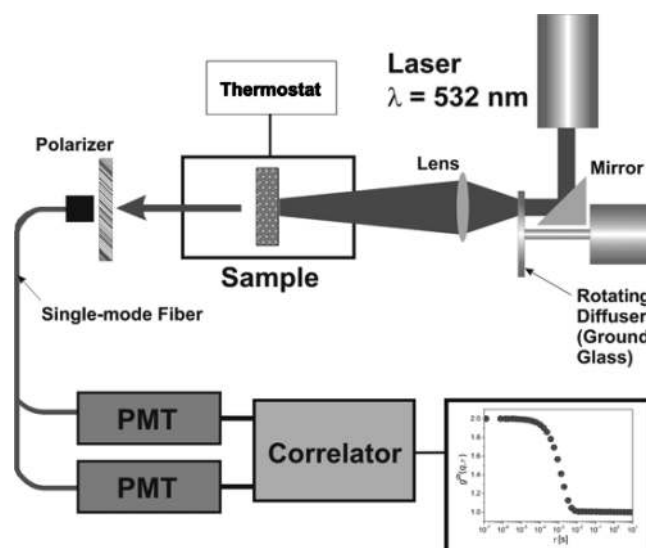


Figure 1. Schematic diagram of our DWS setup. Laser light is scattered from a ground glass rotated by a fast stepper motor, and the transmitted light is collected by a lens to illuminate the sample. A single mode fiber collects the scattered light in transmission. The collected light is subsequently analyzed by a single-photon detector and digital photon counter.

322 from the measured autocorrelation function $g_2(t)$. In our experiments,
323 we added 2% polystyrene sulfonate particles (diameter 720 nm,
324 IDC Corporation, Portland, OR) to the micellar solution temporarily
325 heated to 60 °C in order to reduce the viscosity. The sample was
326 filled in standard glass cuvettes (Hellma) with a path length of 2 mm
327 and a width of 10 mm. The temperature was controlled within ± 0.1
328 °C using a home-built temperature control chamber. A frequency
329 doubled neodymium:yttrium vanadate (Nd:YVO4) laser (Verdi,
330 Coherent) operating at a wavelength $\lambda = 532$ nm was used to illuminate
331 a circular ground glass mounted on a two phase stepper motor
332 (KH42HM2-851 from Japan Servo). Putting a fast rotating diffuser
333 in the optical path between the laser and sample allows for more
334 efficient ensemble averaging.⁵² We collected the transmitted light
335 coming from the ground glass and focused it onto the sample with
336 a spot size diameter of roughly 5 mm. The scattered laser light was
337 then collected using a single-mode optical fiber and single photon
338 counter and subsequently analyzed by using a digital correlator
339 (Correlator.com, NJ). By numerical analysis using eq 11, we extracted
340 the particle mean square displacement $\langle \Delta r^2(t) \rangle$ from the ICF typically
341 over a range of values $g_2 = 0.01 - 0.99$. Figure 1 shows a schematic
342 diagram of our DWS setup.

343 **3.3. Squeeze Flow.** Oscillatory squeeze flow experiments were
344 performed using a piezo-driven axial vibrator (PAV). General theory
345 of squeeze flow is covered in standard textbooks of fluid mechanics.⁵³
346 The theory of the PAV as well as the mechanical and electronic
347 setup are thoroughly discussed elsewhere,^{54,55} and therefore, this is
348 summarized here only briefly. The actor is a thin-walled quadratic
349 copper tube with a thick stainless steel plate on top. Four piezoelectric
350 actuators are attached to two opposite walls of the tube in order to
351 exert the vibrations, and four additional piezoelectric sensors are
352 fixed to the remaining sides in order to pick up the response signal.
353 Direct coupling of excitation and detection is avoided by four partial
354 cuts of the tube parallel to the longitudinal axis. This lower part of
355 the device is surrounded by a double-walled cylinder allowing for
356 circulation of a thermostating fluid, and the temperature is controlled

(42) von Berlepsch, H.; Harnau, L.; Reineker, P. *J. Phys. Chem. B* **1998**, *102*, 7518.

(43) Xu, J.; Tseng, Y.; Carriere, C. J.; Wirtz, D. *Biomacromolecules* **2002**, *3*, 92–99.

(44) Mason, T. G.; Ganesan, K.; van Zanten, J. H.; Wirtz, D.; Kuo, S. C. *Phys. Rev. Lett.* **1997**, *79*, 3282–3285.

(45) Gardel, M. L.; Valentine, M. T.; Crocker, J. C.; Bausch, A. R.; Weitz, D. A. *Phys. Rev. Lett.* **2003**, *91*, 158302.

(46) Maret, G.; Wolf, P. E. *Z. Phys. B: Condens. Matter* **1987**, *65*, 409–413.

(47) Zakharov, P.; Cardinaux, F.; Scheffold, F. *Phys. Rev. E* **2006**, *73*, xxx.

(48) Scheffold, F.; Schurtenberger, P. *Soft Mater.* **2003**, *1*, 139.

(49) Schurtenberger, P.; Stradner, A.; Romer, S.; Urban, C.; Scheffold, F. *CHIMIA: Int. J. Chem.* **2001**, *55*(3), 155–159.

(50) Heinemann, C.; Cardinaux, F.; Scheffold, F.; Schurtenberger, P.; Escher, F.; Conde-Petit, B. *Carbohydr. Polym.* **2004**, *55*(2), 155–161.

(51) Kaplan, P. D.; Kao, M. H.; Yodh, A. G.; Pine, D. J. *Appl. Opt.* **1993**, *32*, 3828.

(52) Zakharov, P.; Cardinaux, F.; Scheffold, F. *Phys. Rev. E* **2006**, *73*, 011413.

(53) Bird, R. B.; Armstrong, R. C.; Hassager, C. *Dynamics of Polymeric Liquids, Vol. 1, Fluid Dynamics*, 2nd ed.; Wiley: New York, 1987.

(54) Crassous, J. J.; Regisser, R.; Ballauff, M.; Willenbacher, N. *J. Rheol.* **2005**, *49*, 851.

(55) Kirschenmann, L. Ph.D. Thesis, Universität Ulm, 2003, p 11.

with an accuracy of ± 0.04 °C. The whole setup is covered by a thick metal lid, which is the upper boundary of the gap and provides a complete sealing for the apparatus. The instrument is operated by a lock-in amplifier. The applied voltage of the driving piezos is proportional to the axial force. The instrument operates at a constant force amplitude F_0 , and from the complex ratio of the dynamic displacement of the lower plate (amplitude ≈ 5 nm) with and without fluid x_f^*/x_0^* one can calculate the complex squeeze stiffness K^* of the fluid using an appropriate mechanical equivalent circuit and solving its equations of motion. In order to calculate K^* from the ratio of the output voltage U/U_0 and the phase difference $\Delta\varphi$ recorded by the lock-in amplifier with and without fluid, the mechanical properties (spring constant mass, resonance frequency) of the instrument itself have to be determined as described in ref 55. Finally, K^* is related to the complex shear modulus G^* and compressibility k_c^* by⁵⁵

$$\frac{1}{K^*} = \frac{2d^3}{3\pi R^4} \left(\frac{1}{G^*} + \frac{3R^2}{2d^2} k_c^* \right) \quad (12)$$

where R (here 10 mm) is the radius and d is the height of the gap. The determination of G^* strongly depends on the exact knowledge of d , which is determined by calibration using Newtonian liquids with viscosities between 1 and 2000 mPas. Gap heights between 15 and 100 μm have been used here. The required sample volume is on the order of 100 μL depending on the height of the gap. Samples have to be degassed carefully in order to avoid artificial compressibility from entrapped air. In principle, the measured G^* values have to be corrected for the k_c^* contribution. For viscoelastic surfactant solutions investigated, here G^* is typically far below 1000 Pa and the compressibility is approximately that of water ($k_{c,w} = 4.6 \times 10^{-10} \text{ Pa}^{-1}$ at 20 °C). Therefore, the corresponding correction to G^* is well below 5% and can thus be safely neglected. Dynamic shear moduli G^* in the range from 0.1 Pa to 10 kPa are accessible.

3.4. Rotational Rheometry. A rotational rheometer Thermo MARS II equipped with a cone-plate measuring cell (diameter $d_{CP} = 35$ mm, cone angle $\alpha_{\text{cone}} = 4^\circ$) was used to perform small amplitude oscillatory shear experiments covering the frequency range from 0.01 to 100 rad/s at a strain amplitude $\gamma_0 = 0.1$. Strain sweep experiments performed prior to the frequency sweeps confirm that this strain amplitude is sufficiently small to provide a linear material response at all investigated frequencies. Measurements were performed at temperatures between 20 and 40 °C. A solvent trap was used to avoid evaporation of the sample during the experiment.

4. Results and Discussion

4.1. Comparison of Mechanical Rheometry and DWS Measurements. The variation of the dynamic shear moduli G' and G'' as a function of frequency as determined from mechanical and optical rheometry has been investigated for the system CPyCl/NaSal at $0.5 < R < 5$. In general, good agreement is found between mechanical and optical methods. Results for $R = 0.6$, corresponding to the first viscosity maximum, have been reported earlier.¹ The shapes of the relaxation spectra from DWS and mechanical rheometry coincide very well over the whole frequency range, but the DWS absolute values of G' and G'' are shifted with respect to the mechanical measurements. The reasons for this shift have already been discussed in ref 1; they can be attributed to uncertainties in experiment as well as residual perturbations of the complex fluid in the particle vicinity⁵⁶ as discussed below. Variations of the zero-shear viscosity η_0 , the terminal relaxation time T_R , and the plateau modulus G_0 as a function of R from mechanical and optical techniques are given in Figure 2. T_R and G_0 are directly deduced from the modulus

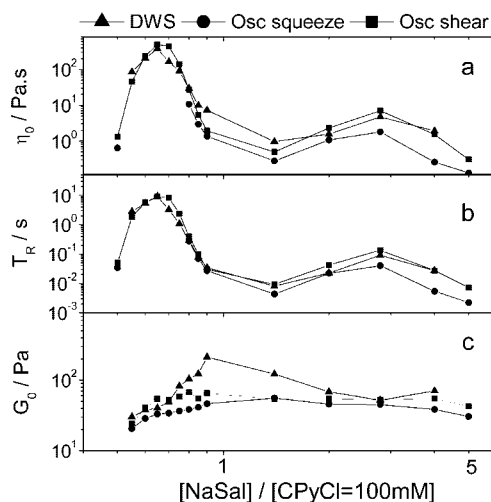


Figure 2. Zero-shear viscosity η_0 (a), terminal relaxation time T_R (b), and plateau modulus G_0 (c) as a function of $R = [\text{NaSal}]/[\text{CPyCl}]$ at constant surfactant concentration of 100 mM CPyCl obtained from DWS (triangles), oscillatory squeeze flow (circles), and rotational rheometry (squares). $T = 20$ °C. All the error bars are as large as the size of the different symbols.

curves. T_R is given by the inverse angular frequency corresponding to the first crossover between G' and G'' . For DWS and oscillatory squeeze flow, G_0 is determined as the value of the modulus G' at the frequency at which G'' has its local minimum, G_{min}'' . For rotational rheometry, G_0 is taken as the value of G' where it exhibits a constant plateau, since the minimum in G'' is not accessible with this technique. The zero-shear viscosity is obtained by using the equation $\eta_0 \approx G_0 T_R$. The first observation is that the variations of η_0 , T_R , and G_0 as a function of R are qualitatively the same values independent of the technique used. Both η_0 and T_R pass through two maxima:² the first maximum occurs at $R \sim 0.65$ and the second at $R \sim 3$. Interpretations of these variations will be discussed below. For T_R , the absolute values are in very good agreement for the different techniques, and the differences are within the experimental error. Concerning the variation of the plateau modulus, the results obtained by rotational rheometry and oscillatory squeeze flow are in good agreement at all salt concentrations investigated. On the contrary, the values of G_0 deduced from DWS measurements show strong deviations (factor 1.5 up to 4.5) from mechanical results in a range of $0.7 < R < 1.4$. A similar result was obtained by Galvan-Miyoshi et al.¹⁵ studying the micellar CTAB/NaSal system. They also compared DWS results with those obtained from mechanical rheometry and found differences between G_0 values increasing with an increase of salicylate concentration. They speculate that large quantities of free ions (Sal^-) in solution are responsible for this behavior. The free ions are not incorporated into the micelles and could therefore modify the mobility of the Brownian particles. This explanation is not valid in our case, because deviations occur at intermediate R values ($0.7 < R < 1.4$) and not at the highest R values. Alternatively, tracer sedimentation was considered to be responsible for these deviations. In that case, the tracer concentration should increase toward the bottom of the cell, and as a consequence the transport mean free path l^* would be underestimated and accordingly G' and G'' would be overestimated. This hypothesis can be rejected, because experimentally all l^* values are around a constant value of 200 ± 30 μm and such differences could not explain a shift factor of 4.5 in the plateau modulus. The compatibility of the tracers and the surrounding medium can be shown by measuring samples with and without tracers mechanically, and we find no measurable

(56) Chen, D. T.; Weeks, E. R.; Crocker, J. C.; Islam, M. F.; Verma, R.; Gruber, J.; Levine, A. J.; Lubensky, T. C.; Yodh, A. G. *Phys. Rev. Lett.* **2003**, *90*, 108301.

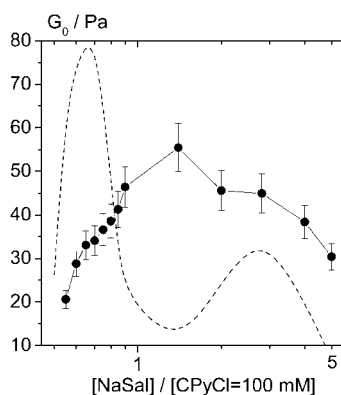


Figure 3. Plateau modulus G_0 (circles) as a function of R obtained from oscillatory squeeze flow measurements at $T = 20^\circ\text{C}$. The dashed line represents the variation of the zero-shear viscosity η_0 in an arbitrary unit.

458 differences within experimental errors. Nevertheless, this not to
 459 exclude that a small fraction of surfactant may adsorb at the
 460 surface of the tracer particles and therefore modify their mobility.
 461 Such an adsorption may have no effect on mechanical measurements
 462 but on DWS results. Aggregation of tracer particles or a
 463 local structure formation hindering tracer motion may be other
 464 possible scenarios which would reduce the plateau value of the
 465 mean square displacement and thus result in an apparent increase
 466 of G_0 . We have no indication for heterogeneity of the solutions
 467 investigated here, since they are all transparent and monophasic
 468 at $T = 20^\circ\text{C}$. Aggregation seems to be an issue; we have observed
 469 significant particle aggregation in aqueous suspensions by visual
 470 inspection in an optical microscope at least for large tracer particles
 471 ($2.3\ \mu\text{m}$ diameter), and typically these aggregates consisted of
 472 2–3 particles. Finally, we have performed DWS measurements
 473 on the system for $R = 0.9$, for which G_0 deviates the most from
 474 mechanical data, using tracers with a larger diameter of $1.3\ \mu\text{m}$.
 475 The shape of the curve is similar to that obtained with the $0.72\ \mu\text{m}$
 476 tracer diameter, but the plateau modulus has decreased from
 477 211 to 100 Pa. This value is still 2 times higher than the mechanical
 478 value (50 Pa), but it seems that the diameter of the tracer particle
 479 may have some effect on the DWS measurements. Particle
 480 aggregation as well as adsorption of surfactant on the tracer
 481 surface is expected to depend on surfactant concentration, ionic
 482 strength, as well as particle size and concentration. This
 483 phenomenon is currently under investigation.

4.2. Effect of Salt on Structural and Dynamic Properties.

484
 485 **4.2.1. Plateau Modulus.** Almost all of the literature dealing with
 486 the linear viscoelastic properties of wormlike micelles are based
 487 on data from small amplitude oscillatory shear experiments
 488 performed by conventional rotational rheometry and are thus
 489 limited to the frequency range $\omega < 100\ \text{rad/s}$. In order to provide
 490 the most accurate data at intermediate frequencies between 10
 491 and $10^4\ \text{rad/s}$, we used oscillatory squeeze flow measurement to
 492 determine the plateau modulus G_0 , which is related to the cross-
 493 link density or mesh size of the entanglement network. In Figure
 494 3, we give the variation of the plateau modulus as a function of
 495 the ionic strength for the system CPyCl/NaSal at a constant
 496 surfactant concentration of 100 mM. The shear modulus varies
 497 significantly with ionic strength. It increases by approximately
 498 a factor of 2 from $R = 0.5$ to 1.4, with the range corresponding
 499 to the first zero-shear viscosity maximum, and then slightly
 500 decreases up to $R = 5$. Cryo-TEM pictures taken for the same
 501 salt/surfactant system, but at a surfactant concentration of 15
 502 mM, clearly show a transition from linear to branched micelles
 503 at the first maximum of zero-shear viscosity, with the branching

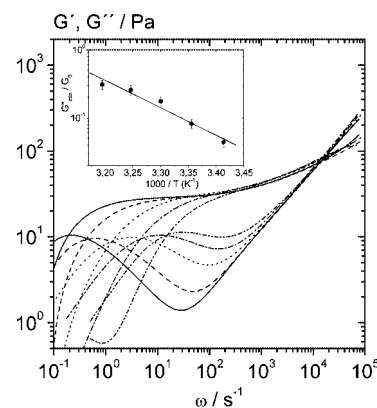


Figure 4. Dynamic shear moduli G' and G'' of an aqueous solution of 100 mM CPyCl/60 mM NaSal as a function of temperature obtained from DWS measurements: 20°C (solid line), 25°C (dashed line), 30°C (dotted line), 35°C (dash-dotted line), 40°C (dash-dotted-dotted line). Inset: Ratio of the minimum value of G'' and the plateau modulus G_0 as a function of $1/T$ for the same solution.

504 density increasing up to the minimum of η_0 .⁴ The increase in G_0
 505 can thus be attributed to the additional contribution of branching
 506 points to the cross-link density. In a previous study performed
 507 at a surfactant concentration of 60 mM,² G_0 was found to be
 508 independent of salt concentration. One possible explanation of
 509 this contradictory observation is that, with 60 mM CPyCl, the
 510 amplitude of the two zero-shear viscosity maxima is about a
 511 factor of 10 lower compared to the system with 100 mM CPyCl.
 512 Accordingly, the contribution of branching points to G_0 is lower
 513 and presumably within experimental uncertainty. The slight
 514 decrease of G_0 for $R > 1.4$ can at least qualitatively be attributed
 515 to a decrease of the branching density accompanied by an increase
 516 of micelle length as shown by the cryo-TEM images taken for
 517 R values in the region of the second η_0 increase. Furthermore,
 518 TEM images for samples with R values corresponding to the
 519 second η_0 maximum show a shortening of the micelles and an
 520 increase of the branching density, but also the formation of
 521 micellar rings is observed. The formation of branching seems
 522 not to compensate the formation of micellar rings, since G_0 further
 523 decreases.

524 **4.2.2. Scission Energy of Wormlike Micelles.** E_{sciss} is calculated
 525 from the temperature dependence of the ratio G_{min}''/G_0 according
 526 to eq 4. The frequency range of oscillatory shear rheometry is
 527 not always sufficient to determine this minimum correctly, but
 528 mechanical squeeze flow gives reliable values for G_{min}''/G_0
 529 and thus allows for an accurate determination of the scission
 530 energy. Figure 4 shows the relaxation spectra from DWS
 531 measurements for the system with $R = 0.6$ at four different
 532 temperatures between 20 and 40°C . The terminal zone and the
 533 Maxwell relaxation frequency ω_r are strongly shifted at higher
 534 frequencies, and the absolute value of G'' around its minimum
 535 at intermediate frequencies strongly increases as temperature is
 536 raised. This directly shows that the micellar contour length \bar{L}
 537 decreases as temperature goes up. The plateau modulus, G_0 , is
 538 almost independent of temperature, which means that the mesh
 539 size ξ of the entanglement network is essentially independent of
 540 temperature, irrespective of the drastic change in \bar{L} . The insert
 541 of Figure 4 represents the variation of G_{min}''/G_0 with $1/T$. E_{sciss}
 542 can be extracted from the slope of this semilogarithmic plot of
 543 G_{min}''/G_0 versus $1/T$. The variation of E_{sciss} as a function of
 544 salt concentration is shown in Figure 5, where values extracted
 545 from DWS and oscillatory squeeze flow are compared. For both

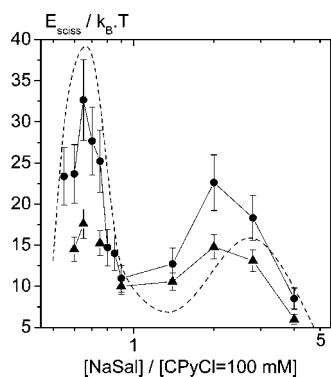


Figure 5. Dependence of scission energy E_{sciss} as a function of R obtained from DWS (circles) and oscillatory squeeze flow (triangles) measurements. The dashed line represents the variation of the zero-shear viscosity η_0 in an arbitrary unit.

546 techniques, E_{sciss} exhibits two maxima analogous to the variation
 547 of the zero-shear viscosity. The first increase in E_{sciss} directly
 548 reveals the increase of the average length of the linear micelles,
 549 which is due to the increasing screening of the electrostatic
 550 repulsions between the charged head groups. This results in a
 551 reduction of the optimal molecular area at the hydrocarbon–water
 552 interface, leading to an increase in the end-cap energy and
 553 accordingly to an increase in average micellar length. The decrease
 554 of E_{sciss} after the first maximum is related to the formation of
 555 branching points.⁴ In that case, the scission energy is related to
 556 the average contour length between branching points \bar{L}_c , and an
 557 increase in the number of branching points will lead to a decrease
 558 in \bar{L}_c , which corresponds to a decrease of the scission energy.
 559 The second increase is again attributed to an increase of the
 560 micellar length \bar{L} , and this is in agreement with the cryo-TEM
 561 images showing a decrease of the branching density accompanied
 562 by an increase of micellar length. And finally, the decrease of
 563 E_{sciss} after the second maximum can be rationalized in terms of
 564 a shortening of the micelles and an increase of the branching
 565 density as again confirmed by cryo-TEM images. In conclusion,
 566 the variation of E_{sciss} directly shows changes in micellar structure
 567 induced by the variation of ionic strength, and the results are
 568 qualitatively in line with the cryo-TEM study on the same salt/
 569 surfactant system performed at lower surfactant concentration.⁴
 570 Finally, it should be noted that the DWS absolute values of E_{sciss}
 571 are about a factor 2 higher compared to the mechanical data. The
 572 reason for this shift is due to deviations in the G_{min}'' DWS data,
 573 especially at temperatures of 20 and 25 °C where $G'' \ll G'$.
 574 Contrary to mechanical measurements, the in- and out-of-phase
 575 contributions are not measured independently in a DWS
 576 experiment but have to be extracted from a single value of the
 577 slope $\delta \ln(\Delta^2(t))/\delta t$. As a consequence, if $G'(\omega)$ and $G''(\omega)$
 578 are of different magnitude, the lower value extracted from DWS
 579 measurements is often not very well defined and here results in
 580 G_{min}'' values much lower than that from mechanical measure-
 581 ments. Consequently, the mechanical measurements are more
 582 appropriate for a determination of absolute values of E_{sciss} .

583 **4.2.3. Persistence Length of Wormlike Micelles.** The persistence
 584 length l_p has been determined from the absolute value of
 585 G^* in the $\omega^{3/4}$ -scaling regime according to eq 7. In order to
 586 obtain more reliable data in the ultrahigh frequency regime (up
 587 to 10^6 rad/s), we applied a simple (self-consistent) correction
 588 scheme to account for inertial effects when the motion of the
 589 tracer particles changes from Brownian to ballistic. The inset of
 590 Figure 6 shows the variations of G' and G'' as a function of
 591 frequency with and without inertial correction. In particular, G'
 592 is strongly modified by this correction and the unphysical

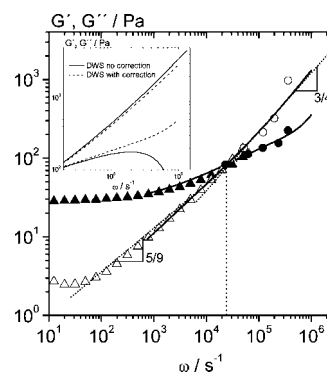


Figure 6. Dynamic shear moduli G' and G'' of an aqueous solution of 100 mM CPyCl/60 mM NaSal at $T = 20$ °C obtained from DWS (solid lines) and various mechanical rheometers (G' , solid symbols; G'' , open symbols): oscillatory squeeze flow (triangles) and torsional resonators from ref 1 (circles). Inset: G' , G'' after inertial correction (dotted lines) of the DWS raw data (solid lines).

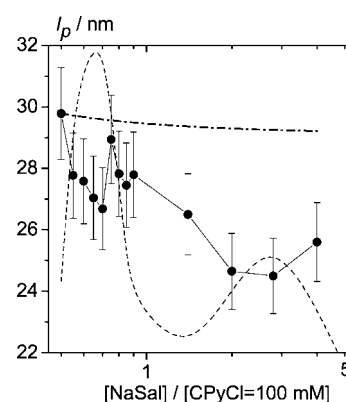


Figure 7. Dependence of persistence length l_p from DWS measurements (circles, 5% error bars) and from OSF theory normalized to the DWS l_p value at $R = 0.5$ (dash-dotted line) as a function of R . The dashed line represents the variation of the zero-shear viscosity η_0 in an arbitrary unit.

593 downward curvature at frequencies $> 10^5$ rad/s is removed and
 594 G' follows the $\omega^{3/4}$ -scaling analogous to G'' . The inertia correction
 595 also modifies G'' , and we have used this data set to calculate l_p ,
 596 since the $\omega^{3/4}$ -scaling is more evident and extends over a broader
 597 frequency range in G'' than in G' . We fit the function $G'' =$
 598 $k_{\text{DWS}}\omega^{3/4}$ to the experimental data and calculate l_p from the
 599 resulting k_{DWS} value according to eq 7. This equation requires a
 600 lateral drag coefficient $\delta = 4\pi\eta_s/\ln(0.6\lambda/d_{\text{mic}})$. The characteristic
 601 length λ is set equal to the mesh size, η_s is the solvent viscosity,
 602 and for the micelle diameter we insert $d_{\text{mic}} = 2.6$ nm.³⁹ This
 603 results in $\delta = 0.005$ N s/m². Figure 7 shows the variation of l_p
 604 as a function of salt concentration from DWS measurements.
 605 We observe a decrease of l_p from ~ 30 to ~ 26 nm over the total
 606 range of salt concentration investigated. Obviously, the linear-
 607 to-branched transition does not have a significant effect on l_p ,
 608 and this increase in flexibility is considered to be an ionic strength
 609 effect due to the screening of electrostatic repulsion. In order to
 610 verify this assumption, we compared our results with the
 611 predictions of the OSF theory. According to this theory, for
 612 charged systems such as ordinary polyelectrolytes or wormlike
 613 micelles of ionic surfactants, the persistence length l_p can be
 614 expressed as a sum of an intrinsic component $l_{p,0}$ and an
 615 electrostatic component $l_{p,e}$.^{58,59}

(58) Odijk, T. J. *Polym. Sci., Polym. Phys. Ed.* **1977**, *15*(3), 477–483.

(59) Skolnick, J.; Fixman, M. *Macromolecules* **1977**, *10*(5), 6717–6727.

$$l_p = l_{p,0} + l_{p,e} \quad (13a)$$

and the electrostatic contribution $l_{p,e}$ is given by

$$l_{p,e} = \frac{1}{4\kappa^2 l_B} \quad (13b)$$

with the Bjerrum length $l_B = 0.71$ nm and the Debye length κ^{-1} (nm) = $0.304/(C_{\text{salt}})^{1/2}$.

This electrostatic contribution has been investigated in various surfactant/salt systems,^{29,60–62} but in the majority of cases no systematic investigations have been performed comparing experimental results for l_p and predictions of OSF theory. Schurtenberger et al.⁵⁹ made such a comparison for the system composed of nonionic hexaethylene glycol mono-*n*-hexadecyl ether ($C_{16}E_6$) “doped” with a small amount of ionic surfactant 1-hexadecane sulfonic acid ($C_{16}SO_3Na$) in the presence of nonpenetrating counterion (NaCl). They found that $l_{p,e}$ absolute values were significantly higher than those predicted by the OSF theory, but they were not able to explain this systematic deviation. For the system investigated here, the variation of the persistence length l_p^{OSF} calculated from eq 13b is given in Figure 7. This electrostatic contribution is very small; l_p^{OSF} decreases by less than 1 nm in all the salt ranges investigated. Despite the experimental uncertainty of the l_p^{DWS} values, their decrease is significantly stronger than that predicted by OSF theory. Similar observations were obtained by Galvan-Miyoshi et al.¹⁵ for the system CTAB/NaSal. Schubert et al.¹¹ also found a strong decrease of the persistence length with increasing salt for a mixed cationic/anionic micellar solution composed of cetyl trimethylammonium tosylate (CTAT) and sodium dodecyl benzyl sulfonate (SDBS) with added Na tosylate penetrating salt. The dependence on ionic strength follows the κ^{-2} -scaling predicted by OSF theory, but again the absolute values are much larger than expected by OSF theory. We assume that the increase in flexibility is due to the incorporation of more and more penetrating salicylate ions as R increases. Indeed, the penetration into the interior of the micelle by the salicylate ions can reverse the charge of the micelle from positive to negative, involving changes of dynamical properties, and can be responsible for the stronger increase in flexibility compared to the electrostatic contribution. In order to further elucidate this phenomenon, a similar study using a system with nonpenetrating counterions is in progress.

Finally, using our l_p^{DWS} experimental values, we calculated the contour length L of the micelles from the equations (G_{min}''/G_0) $\approx (le/\bar{L})$ with $le \approx \xi^{5/3} l_p^{2/3}$ and $\xi = (k_B T/G_0)^{1/3}$. Figure 8 shows the dependence of \bar{L} as a function of R . \bar{L} exhibits two maxima analogous to the scission energy, and this result confirms the findings on E_{sciss} in section 4.2.2 and demonstrates the consistency of our data analysis.

5. Conclusion

The system CPyCl/NaSal is known to exhibit two maxima in zero-shear viscosity as the salt concentration is varied.² The

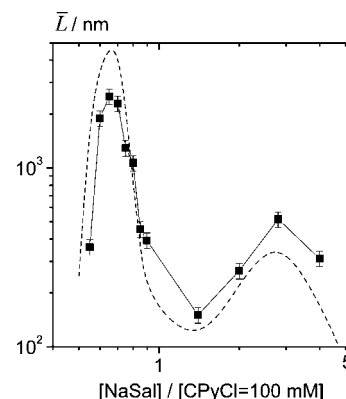


Figure 8. Dependence of the contour length \bar{L} as a function of R obtained from DWS (squares). The dashed line represents the variation of the zero-shear viscosity η_0 in an arbitrary unit.

different viscosities are a result of structural changes as confirmed by cryo-TEM imaging.⁴ At low salt concentration, the micelles are linear and their average contour length increases with increasing ionic strength. The first viscosity maximum corresponds to a transition from linear to branched micelles. The second viscosity increase corresponds to a decrease of the branching density accompanied by an increase of micelle length, and the second viscosity maximum to a shortening of the micelles with an increase of the branching density. With further increase of salt concentration, the formation of micellar rings is also observed. We have used various mechanical techniques as well as DWS optical microrheology to characterize the linear viscoelastic properties of this surfactant/salt system in a broad frequency range from 0.01 up to 10^6 s⁻¹. At a fixed surfactant concentration of 100 mM, we varied the salt/surfactant ratio R from 0.5 to 4. From these dynamic measurements, we can directly determine important structural features such as the cross-link density of the entanglement network, the scission energy, and the persistence length l_p . The persistence length l_p decreases monotonically with increasing salt concentration. This decrease is stronger than that predicted by the OSF theory which takes into account electrostatic screening effects. We attribute this to an additional increase in micellar flexibility due to the strongly binding salicylate counterion, which is known to penetrate into the micelles. This will be further investigated by a comparative study using a nonpenetrating counterion. The transition from linear to branched micelles obviously has no significant influence on l_p . The plateau modulus G_0 increases at the linear-to-branched micelles transition, and this is attributed to the additional contribution of branching points to the cross-link density. The scission energy E_{sciss} exhibits two maxima analogous the zero-shear viscosity, which can be understood in terms of the variation of micellar length and variation of the amount of branched micelles and contour length between branching points.

Acknowledgment. The authors thank D. Danino (Department of Biotechnology and Food Engineering, Technion, Haifa, Israel) for providing unpublished results of her cryo-TEM experiments and for fruitful discussions.

(60) Sommer, C.; Pedersen, J. S.; Egelhaaf, S. U.; Cannavacciuolo, L.; Kohlbrecher, J.; Schurtenberger, P. *Langmuir* **2002**, *18*, 2495–2505.

(61) Cannavacciuolo, J.; Pederson, S.; Schurtenberger, P. *Langmuir* **2002**, *18*, 2922–2932.

(62) Magid, L. J.; Han, Z.; Li, Z.; Butler, P. D. *J. Phys. Chem. B* **2000**, *104*(29), 6717–6727.